The Plant Cell, Vol. 28: 2478–2492, October 2016, www.plantcell.org

The Developmental Regulator SEEDSTICK Controls Structural and Mechanical Properties of the Arabidopsis Seed Coat

Ignacio Ezquer,[a,b] Chiara Mizzotti,[a] Eric Nguema-Ona,[c,d] Maxime Gotté,[c] Léna Beauzamy,[e] Vivian Ebeling Viana,[f] Nelly Dubrulle,[e] Antonio Costa de Oliveira,[f] Elisabetta Caporali,[a] Abdoul-Salam Koroney,[c] Arezki Boudaoud,[e] Azeddine Driouich,[c] and Lucia Colombo[a,b,1]

[a] Dipartimento di BioScienze, Università degli Studi di Milano, 20133 Milan, Italy
[b] Consiglio Nazionale delle Ricerche, Istituto di Biofisica, 20133 Milan, Italy
[c] Laboratoire Glycobiologie et Matrice Extracellulaire, Normandie Université, UNIROUEN, Végétal, Agronomie, Sol, et Innovation (VASI), 76821 Mont-Saint-Aignan, France
[d] Centre Mondial de l'Innovation-Laboratoire de Nutrition Végétale, 35400 Saint Malo, France
[e] Laboratoire de Reproduction et Développement des Plantes, INRA, CNRS, ENS, UCB Lyon 1, Université de Lyon, 69364 Lyon Cedex 07, France
[f] Plant Genomics and Breeding Center, Technology Development Center, Federal University of Pelotas, RS 96010-900, Brazil

ORCID IDs: 0000-0003-1886-0095 (I.E.); 0000-0003-3644-2890 (C.M.); 0000-0002-0292-9273 (E.N.-O.); 0000-0001-7192-0945 (M.G.); 0000-0002-8326-7549 (V.E.V.); 0000-0002-4869-2451 (N.D.); 0000-0001-8835-8071 (A.C.d.O.); 0000-0002-2780-4717 (A.B.); 0000-0001-7032-6047 (A.D.); 0000-0001-8415-1399 (L.C.)

Although many transcription factors involved in cell wall morphogenesis have been identified and studied, it is still unknown how genetic and molecular regulation of cell wall biosynthesis is integrated into developmental programs. We demonstrate by molecular genetic studies that SEEDSTICK (STK), a transcription factor controlling ovule and seed integument identity, directly regulates *PMEI6* and other genes involved in the biogenesis of the cellulose-pectin matrix of the cell wall. Based on atomic force microscopy, immunocytochemistry, and chemical analyses, we propose that structural modifications of the cell wall matrix in the *stk* mutant contribute to defects in mucilage release and seed germination under water-stress conditions. Our studies reveal a molecular network controlled by STK that regulates cell wall properties of the seed coat, demonstrating that developmental regulators controlling organ identity also coordinate specific aspects of cell wall characteristics.

INTRODUCTION

It is commonly accepted that the mechanisms of patterning and growth are tightly constrained by genetic regulation and that this constitutes the basis of morphogenesis. Although molecular approaches continue to reveal genetic mechanisms of pattern formation, the link between genetic regulators and global shape control remains a central question in developmental biology. Among the factors that contribute to the final shape of a given tissue or organ, the cell wall plays a significant role (Lodish et al., 2000). Indeed, the spatial-temporal patterning of growing tissues is governed by a complex regulatory network controlling the composition, organization, and mechanical properties of the cell wall (Boudon et al., 2015). Cell wall-modifying enzymes, such as expansins and xyloglucan endotransglycosylases, and pectin-modifying enzymes, including pectin methylesterases (PMEs) and PME inhibitor (PMEI) proteins, play roles in cell wall reorganization (Peaucelle et al., 2012). Genes involved in cell wall modification act downstream of transcription factors that control plant morphogenesis, such as AINTEGUMENTA (Krizek et al., 2016), APETALA2 (Yant et al., 2010), MONOPTEROS (Schlereth et al., 2010), and AGAMOUS (Gómez-Mena et al., 2005). The activities of such enzymes modulate cell wall composition and components, which in turn affect the viscosity/rigidity of the cell wall. The consequent alterations in extensibility influence growth (Cosgrove, 2014), as growth by cell elongation involves an irreversible increase in cell volume along with relaxation of the cell wall. The biochemical processes involved in cell wall loosening during growth extension are only partially understood (Keegstra, 2010; Cosgrove, 2014); however, many physiological processes occurring during plant development have already been associated with cell wall-modifying enzymes, such as PMEs (reviewed in Pelloux et al., 2007).

The seed coat protects the embryo and plays important roles in dormancy, dispersal mechanisms, and longevity (Windsor et al., 2000; Bueso et al., 2014). In *Arabidopsis thaliana*, the seed coat is derived from the ovule inner and outer integuments (Haughn and Chaudhury, 2005; Skinner et al., 2004). Upon fertilization, cells from the two layers of the outer integument and the three layers of the inner integument undergo rapid growth. During the first few days after fertilization, this growth entails both cell division and expansion (Windsor et al., 2000). The five different layers follow distinct fates (Haughn and Chaudhury, 2005): The cells of the innermost layer (the endothelium) biosynthesize proanthocyanidins, flavonoid compounds that later oxidize and impart the typical

[1] Address correspondence to lucia.colombo@unimi.it.
The author responsible for distribution of materials integral to the findings presented in this article in accordance with the policy described in the Instructions for Authors (www.plantcell.org) is: Lucia Colombo (lucia.colombo@unimi.it).
www.plantcell.org/cgi/doi/10.1105/tpc.16.00454

brown color to the seed coat (Pourcel et al., 2005; Mizzotti et al., 2014). The apoplast of the outermost layer (also called the mucilage secretory cell) accumulates pectinaceous mucilage (Haughn and Chaudhury, 2005; Western et al., 2000, North et al., 2014). Mucilage formation by the epidermal seed coat layer is a characteristic of several flowering plants (including many of agricultural value) that has attracted attention as a useful genetic model for studying aspects of cell wall biogenesis, function, and regulation (Yang et al., 2012; Western, 2012). Upon extrusion, mucilage is organized into two distinct domains: an inner, dense mucilage tightly attached to the seed and an outer, water-soluble, more diffuse mucilage that can be easily extracted (Macquet et al., 2007; North et al., 2014). Mutations in genes coding for biosynthetic enzymes involved in the production of cell wall polysaccharides cause defects in mucilage release upon hydration (Griffiths et al., 2015; reviewed in North et al., 2014). The potential for studies using Arabidopsis seed coat mucilage as a model for genetic analysis of plant cell wall structure and function has grown substantially in recent years and has been useful in establishing connections between carbohydrate structure and biosynthesis and in vivo cell wall properties (Francoz et al., 2015; Haughn and Western, 2012).

Although mucilage is not required for seed germination under normal conditions, it does provide ecological advantages under extreme conditions by facilitating water imbibition, adherence to soil particles, and the maintenance of adequate moisture (Western et al., 2000; Yang et al., 2012). The release of mucilage is critical in allowing germination under drought conditions as evidenced by the low germination efficiencies under arid conditions of decreased-mucilage mutants, such as *myb61*, *transparent testa glabra1* (*ttg1*), *glabra2* (*gl2*), the bifunctional β-D-xylosidase/α-L-arabinofuranosidase mutant (*bxl1*), and the subtilisin-like serine protease mutant (*sbt1.7*) (Penfield et al., 2001; Willats et al., 2001; Rautengarten et al., 2008; Arsovski et al., 2009). In addition, a correlation between mucilage formation and seed longevity has recently been discovered (Bueso et al., 2014).

One of the major regulators of ovule and seed differentiation is SEEDSTICK (STK), a MADS transcription factor that, along with SHATTERPROOF1 (SHP1) and SHP2, controls ovule integument identity. *STK*, in association with another MADS domain gene *ARABIDOPSIS* B_{SISTER}, is required for correct formation of the endothelium, the innermost layer of the seed coat (Mizzotti et al., 2012). *STK* controls proanthocyanidin metabolism in the seed coat by regulating the expression of *BANYULS*/*ANTHOCYANIDIN REDUCTASE* (*BAN*), which encodes a key enzyme in proanthocyanidin biosynthesis (Mizzotti et al., 2014). Interestingly, *STK* also represses the expression of seed coat regulators, such as *TRANSPARENT TESTA8* (*TT8*) and *ENHANCER OF GLABRA3*, by binding directly to the promoters of these members of the WD40-bHLH-MYB complex (Mizzotti et al., 2014). These factors not only control the biosynthesis of anthocyanin in the endothelial layer of the developing seed coat but also regulate outer seed coat differentiation, consistent with their expression in the developing testa epidermis (Baudry et al., 2006).

It is unclear how mechanical and biochemical changes in seed coat properties (which ultimately lead to testa formation) influence seed coat functions. Here, we show that the role of the homeotic gene *STK* in differentiation hinges on the control of cell wall structure. We discovered that modification of the biogenesis of cell wall components in *stk* mutants altered the mechanical properties of the seed coat, strongly affecting mucilage extrusion and consequently germination under arid conditions. The model we present integrates molecular, biochemical, and mechanical elements to provide a more complete view of the role of developmental regulators in the differentiation of the cell wall.

RESULTS

The *stk* Mutant Shows Reduced Germination Efficiency and Changes in the Cell Wall Mechanical Proprieties

STK plays a pivotal role in the differentiation of ovule and seed integuments (Favaro et al., 2003; Pinyopich et al., 2003; Mizzotti et al., 2012, 2014). Upon fertilization, *STK* is expressed in the outer three cell layers of the seed integuments until the heart embryo stage (Mizzotti et al., 2014; Figure 1A), whereas at later stages (up to linear stage), *STK* expression is limited to the outermost cell layer (Figures 1B and 1C).

The cells of this layer are responsible for the biosynthesis and release of the mucilage upon water imbibition (Figures 1D and 1E). The use of ruthenium red staining indeed revealed the presence of a thick, pink-staining capsule of mucilage around wild-type seeds upon water imbibition (Figure 1D), while *stk* seeds showed a significant reduction (or even absence) of mucilage release (Figure 1E). Wild-type and *stk* seeds were treated with EDTA, which chelates calcium ions and thus facilitates mucilage extrusion (Rautengarten et al., 2008). EDTA treatment caused mucilage extrusion in both wild-type (Figure 1F) and *stk* seeds (Figure 1G).

We imaged the surface of dry, water-imbibed, or EDTA-treated seeds by scanning electron microscopy (Figures 1H to 1M). In dry *stk* seeds, the size of the epidermal cells was reduced compared with the wild type, but no other morphological differences were apparent (Figure 1K). After water imbibition, deep hollows were visible around the columellae of wild-type epidermal cells (Figure 1I), whereas no significant change in seed coat morphology occurred in *stk* cells (Figure 1L), indicating that mucilage had not been extruded in the latter. By contrast, EDTA imbibition caused mucilage release in both wild-type and *stk* seeds and no significant differences were noted in cell morphology between the two (Figures 1J and 1M). Despite this defect in mucilage release, seed coat epidermal cell development, including the formation of columellae and mucilage accumulation in the *stk* mutant, was similar to the wild type (Supplemental Figure 1). Since the hygroscopic properties of mucilage could alter water uptake during germination under conditions of decreased water potential (reviewed in Western, 2012), we tested germination under water stress in wild-type and *stk* seeds (Figures 2A and 2B). Inhibition of germination under water-limiting stress conditions was observed for wild-type seeds exposed to 21% polyethylene glycol (PEG) (Figure 2A). Germination and seedling establishment in *stk* seeds were significantly inhibited on media containing 18% PEG (Figure 2B). Under these conditions, *stk* seeds displayed 60% germination compared with 90% for wild-type seeds. This indicates that altered *stk* seed coat properties influence negatively the sensitivity to water stress.

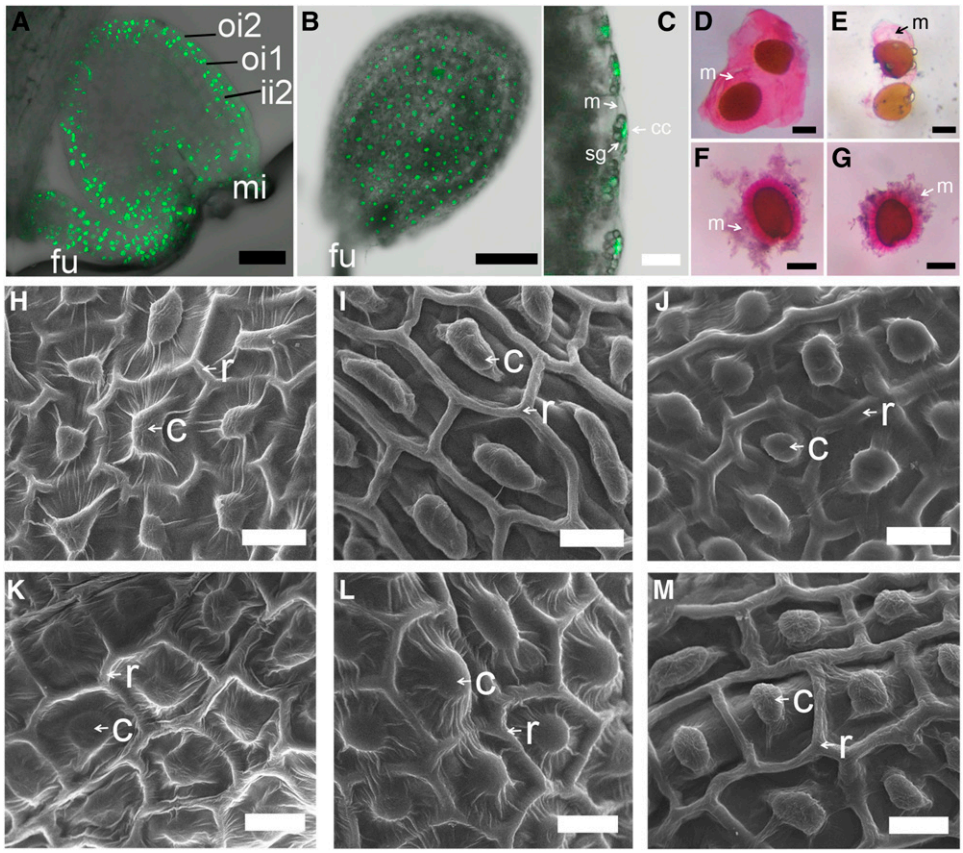

Figure 1. Visualization of *pSTK:STK-GFP* Fluorescence, Water- and EDTA-Treated Seed Mucilage Extrusion, and Seed Surface Morphology.

(A) to **(C)** Confocal laser scanning imaging of the *pSTK:STK-GFP* line: seeds at preglobular **(A)** and linear (**[B]** and **[C]**) cotyledon stage. The STK-GFP signal is expressed in seed outer integuments upon fertilization till 2 DAP **(A)** and only in the epidermal outer layer of the seed coat up to 6 DAP (**[B]** and **[C]**).
(D) to **(G)** Whole-mounted wild-type (**[D]** to **[F]**) and *stk* (**[E]** to **[G]**) mutant seeds stained with ruthenium red. Seeds were treated with water (**[D]** and **[E]**) and EDTA (**[F]** and **[G]**). *stk* mutant seeds are defective in mucilage extrusion.
(H) to **(M)** Scanning electron microscopy of dried and water- and EDTA-treated wild-type and *stk* mutant seeds.
(H) and **(K)** Surface of dried wild-type **(H)** and *stk* mutant **(K)** seeds.
(I) and **(L)** Water-imbibed wild-type **(I)** and *stk* mutant **(L)** seeds.
(J) and **(M)** EDTA-imbibed wild-type **(J)** and *stk* mutant **(M)** seeds.
mi, micropyle; fu, funiculus; ii2, inner integument; oi1 and oi2, outer integuments; m, mucilage; cc, cytoplasmic column; sg; starch grains; c, columella; r, radial cell wall. Bars = 30 μm in **(A)** and **(D)** to **(G)**, 150 μm in **(B)**, and 20 μm in **(C)** and **(H)** to **(M)**.

The biophysical properties of the cell wall could influence the mechanical rupture of the seed coat upon water imbibition. To test whether the mechanical properties of *stk* epidermal cells were modified with respect to the wild type, we took advantage of recent advances in atomic force microscopy (AFM) that have provided insights into the mechanics of plant growth and development (Peaucelle et al., 2012). We used AFM to monitor mechanical changes in the epidermal cells of developing seeds (Supplemental Figure 2; see Methods). Since we found no delay in seed coat development between the *stk* mutant and wild-type seeds (Supplemental Figure 1), we directly compared the mechanical changes in wild-type and *stk* seeds at 2 and 11 d after pollination (DAP). Wild-type seeds showed an apparent elastic modulus mean value of 0.66 ± 0.35 MPa, and a mean value for *stk* seeds of 3.98 ± 1.11 MPa, at 2 DAP (Figure 2C). When we analyzed changes in the nanomechanical properties of the seed cell wall at later stages of seed development (11 DAP), wild-type seeds had an apparent elastic modulus mean value of 23.2 ± 18 MPa and a mean value for *stk* seeds of 44.5 ± 17 MPa (Supplemental Figure 2D).

Our observations indicate that epidermal cell wall stiffness increases as seed growth and maturation proceeds and that the outer layer of the *stk* seed coat is stiffer than that of the wild type.

STK Directly Regulates *PMEI6* Expression

Defects in mucilage extrusion are often linked to modified levels of methylesterification of the homogalacturonans (HGs), one of the mayor components of seed mucilage (North et al., 2014). Therefore, we analyzed the HG methylesterification in *stk* mucilage by immunolabeling using the monoclonal antibodies LM19 and LM20 (Figures 3A to 3H), which recognize poorly methylesterified and highly methylesterified HGs, respectively.

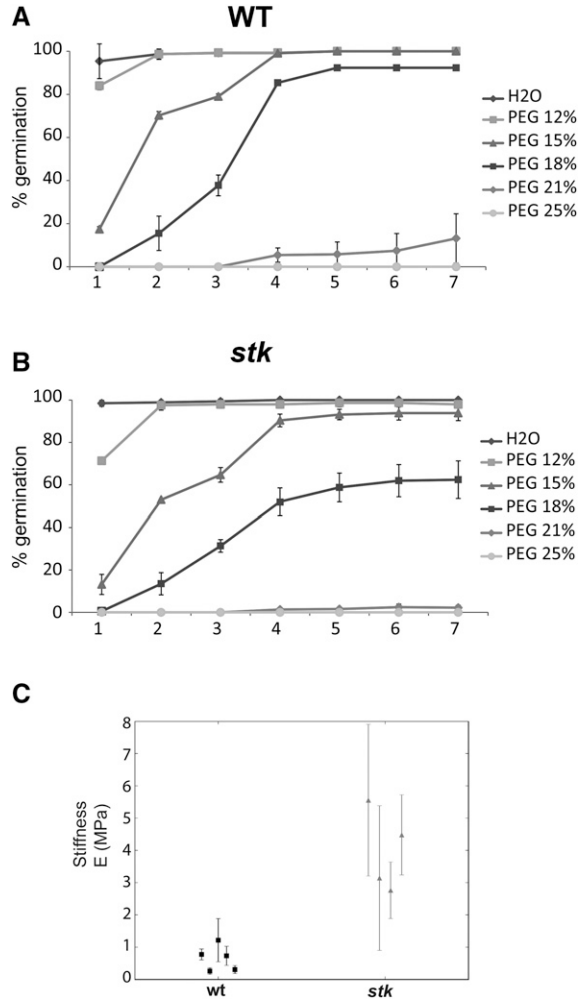

Figure 2. Effects of *stk* Mutation on Seed Germination and Stiffness of the Epidermal Cell Walls of the Seed.

(A) and **(B)** Comparison of the germination rate of wild-type **(A)** and *stk* **(B)** seeds in increasing concentrations of PEG over a 7-d time course. Data points represent the average and SD of three independent experiments in both panels.

(C) Average elastic moduli of the epidermal cell walls of developing wild-type and *stk* seeds. Each square represents the average elastic modulus of over 300 force curves per seed at 2 DAP, allowing the computation of an average apparent elastic modulus and its SD. The horizontal axis differentiates replicates in each genotype (wild type and *stk*). These moduli most likely account for the properties in the direction perpendicular to the cell wall (see Methods).

In wild-type seeds, LM19 antibodies revealed poorly methylesterified HGs distributed along the ray structures in the inner region of the adherent mucilage (Figures 3A and 3B). By contrast, the LM20 immunosignal was visible at the outer edges of the outer mucilage and around the cell walls, which are likely associated with cellulose-enriched columellae (Figure 3E). Neither LM19 nor LM20 signal was present in *stk* seeds treated with water (Figures 3C and 3G). When we treated *stk* seeds with EDTA (Figures 3D and 3H) to facilitate mucilage extrusion (as described in Figure 1), LM19 signal was visible in the outer edges of the outer mucilage but with less intensity than in wild-type seeds, and the labeling along the ray structures in the inner region (observed in wild-type seeds) was absent (compare Figure 3D with 3B). There was no signal from LM20 antibodies in either water- or EDTA-treated *stk* seeds (compare Figure 3E with 3G and 3F with 3H), suggesting the absence of highly methylesterified HGs in the mutant.

To confirm that STK is involved in the modulation of the HG methylesterification, we compared PME activity in the *stk* mutant seeds with that in the wild type using the method of Klavons and Bennett (1986) (Figure 3I). We found that PME activity in *stk* extracts was 25% higher than in the wild type. A higher level of PME activity in *stk* seed extracts was also observed when we compared the diameter and intensity of activity halos by specific gel diffusion assays (Figure 3J). One of the best-characterized enzymes controlling HG methylesterification is PMEI6 (Saez-Aguayo et al., 2013). To explore whether *PMEI6* expression was under the control of STK, we crossed the *pPMEI6:PMEI6-GFP* reporter line (Saez-Aguayo et al., 2013) with the *stk* mutant and analyzed the surface (epidermal cells) of F2 seeds at the bent cotyledon stage (Figure 4A). While the line expressing GFP-tagged PMEI6 in the wild-type background showed GFP activity in the seed epidermis, no signal was detected in the *stk* mutant background (Figure 4A). These observations were further confirmed by qRT-PCR analysis, which showed that *PMEI6* expression was strongly reduced in the *stk* siliques compared with those of the wild type (Figure 4B). These data suggest that *STK* positively regulates *PMEI6*.

To investigate whether the defect in mucilage extrusion in *stk* was due to the lack of PMEI6, we crossed the *stk* mutant with an Arabidopsis line expressing the *PMEI6* CDS under the control of the 35S promoter. As show in Figure 4C, the mucilage release in water imbibition was partially restored, showing that the restoration of *PMEI6* expression in the *stk* mutant could partially complement the mucilage extrusion phenotype.

To understand whether STK, a MADS domain transcription factor, could directly regulate *PMEI6*, we analyzed the sequence for the presence of MADS domain CArG-box binding sites (Tilly et al., 1998). Five putative CArG-boxes were identified (Figure 4D). Subsequently we performed a ChIP (chromatin immunoprecipitation) assay using GFP antibodies and developing siliques (up to 6 DAP) of *stk* mutant plants expressing pSTK:STK-GFP (Figure 4D). Chromatin extracted from wild-type siliques was used as a negative control, and as positive control we monitored the binding of STK to the VERDANDI (VDD) promoter (Matias-Hernandez et al., 2010). Of the five CArG-boxes in the *PMEI6* promoter, the ChIP-qRT assay revealed significant enrichment for binding to the regions spanning CArG-boxes 1 and 2 and CArG-box 4 (Figure 4D).

The Role of STK in Cell Wall Structure and Function

Cellulose is a constitutive component of the seed coat epidermal cell wall and interacts with other polymers, such as HGs, rhamnogalacturonans, and glucomannans, present in the mucilage, thus influencing the properties of the extruded mucilage (Macquet et al., 2007; Mendu et al., 2011; Sullivan et al., 2011; Yu et al., 2014). To determine whether loss of *STK* function affects cellulose deposition and organization as well as its biosynthesis in

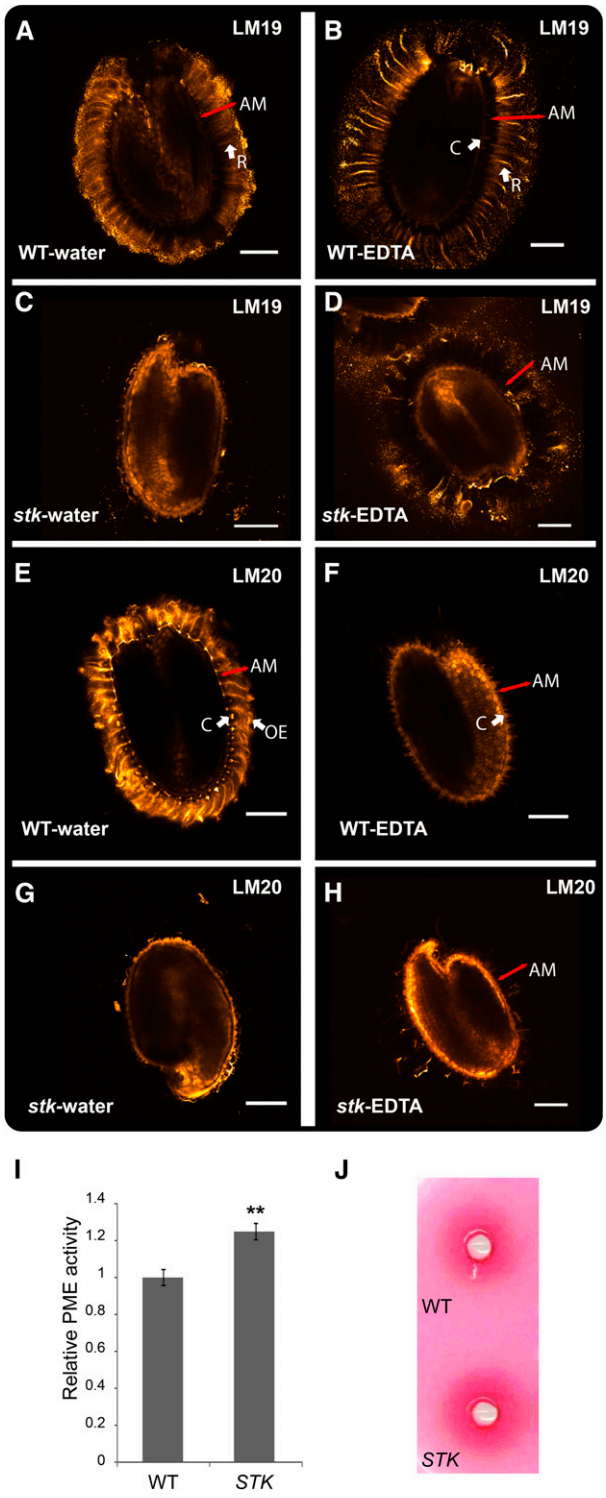

Figure 3. STK Modifies HG Methylesterification and PME Activity in Mucilage Secretory Cells.

(A) to **(H)** Immunolabeling of partially nonesterified and methylesterified HG inner adherent mucilage released from wild-type and *stk* seeds visualized by confocal microscopy (fire colored signal). Whole-mounted mature seeds imbibed in water (**[A]**, **[C]**, **[E]**, and **[G]**) and EDTA (**[B]**, **[D]**, **[F]**, and **[H]**) were labeled with monoclonal antibodies LM19 (**[A]** to **[D]**) and LM20 (**[E]** to **[H]**), which recognize nonesterified or poorly methylesterified HGs and highly methylesterified HGs, respectively. AM, adherent mucilage; R, ray structure; C, columella. Bars = 100 μm.

(I) PME activities in protein extracts from mature wild-type and *stk* dry seeds. PME activity was determined by quantification of formaldehyde produced from methanol by alcohol oxidase, according to Klavons and Bennett (1986). Error bars represent SD ($n = 5$). **, Wilcoxon signed rank test, $P < 0.01$.

(J) Radial gel diffusion assay showing PME (fuchsia halo) activities in proteins extracted from seeds. Equal protein samples (4 μg in 20 μL) were loaded in 4-mm-diameter wells and PME levels were visualized with 0.05% ruthenium red staining.

Arabidopsis mucilage secretory cells, wild-type and *stk* seeds were stained with Calcofluor (which stains cellulose and other β-glucans) and with Pontamine Fast Scarlet 4BS, a cellulose-specific dye (Anderson et al., 2010) (Figures 5A to 5D and 5E to 5H, respectively). In wild-type water-treated seeds, both Calcofluor and Pontamine stained the columellae, the primary cell wall remnants attached to the columellae, and the diffuse rays extending from the tip of the columellae across the adherent layer of the seed mucilage (Figures 5A and 5E, respectively). Following imbibition with EDTA in *stk* seeds, Calcofluor and Pontamine stains showed the diffuse rays, but the staining signal was mostly located at the base of the rays just above the columellae. No tangential cell wall remnants were observed attached to the columellae tips. The naked columellae in *stk* seeds lacked the attached cellulosic fragments that were present in the wild type (compare Figure 5B with 5D and 5F with 5H).

CELLULOSE SYNTHASE5 (CESA5) is required for the production of seed mucilage cellulose and the adherent mucilage (Harpaz-Saad et al., 2011). CESA5 also functions with CESA2 and CESA9 in seed coat epidermal radial wall reinforcement (Mendu et al., 2011; Sullivan et al., 2011). In addition, *cesa3* mutants exhibit altered biosynthesis of mucilage cellulose (Griffiths et al., 2015). *CESA5* transcript levels were markedly decreased in the *stk* mutant, while *CESA2* and *CESA3* expression was slightly enhanced (Figure 5I). We also quantified the expression of *FEI2* and *SOS5*, which play roles in seed mucilage ray formation (Harpaz-Saad et al., 2011). Like *CESA5*, low transcript levels of *FEI2* were found in the *stk* mutant, while the expression of *SOS5* was unaltered (Figure 5I).

The question remains: How do STK-induced transcriptional changes affect overall cellulose deposition in seeds? Therefore, we quantified the crystalline cellulose content of mature Arabidopsis seeds using the Updegraff assay (Updegraff, 1969). Our results indicated a 15% reduction in cellulose levels in *stk* mutant seeds compared with the wild type (Figure 5J).

We have also analyzed the expression of *COBRA-LIKE2* (*COBL2*) and *CELLULOSE SYNTHASE-LIKE A2* (*CSLA2*) because both *cobl2* and *csla2* mutants show malformed rays of cellulose, which ultimately leads to altered adhesion of seed mucilage pectins (Yu et al., 2014; Ben-Tov et al., 2015). In the *stk* mutant, levels of *COBL2* mRNA were unaltered, but those of *CSLA2* were slightly increased (Figure 5I). In the *csla2* mutant, decreased levels of glucomannan lead to a modification of the mucilage cellulose ultrastructure, which affects the maintenance of adherence of the mucilage layer (Yu et al., 2014). We therefore tested whether STK

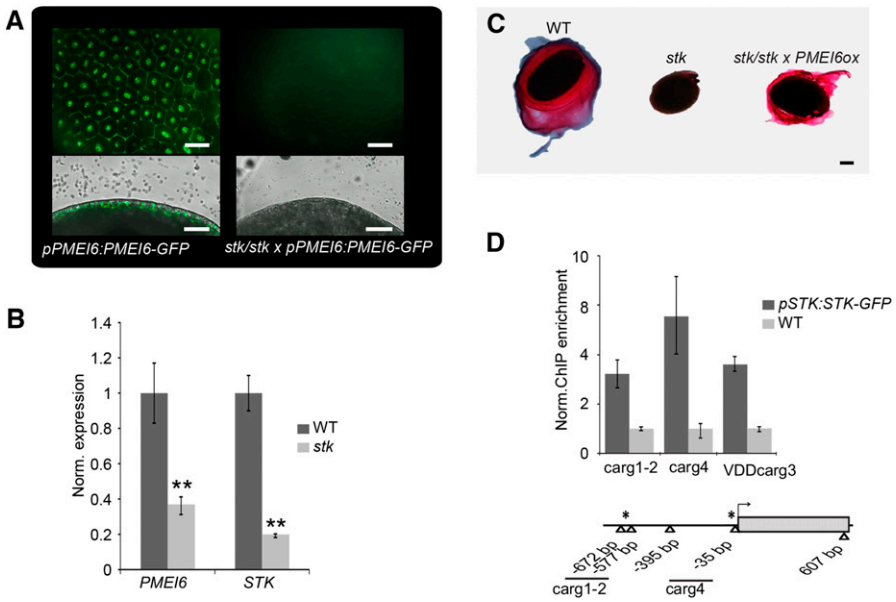

Figure 4. STK Directly Regulates *PMEI6*.

(A) Confocal laser scanning imaging of wild-type and *stk* seeds expressing *pPMEI6:PMEI6-GFP* at the bent cotyledon stage. Fusion protein is visible and expressed in the epidermal outer layer of the wild-type seed coat. This signal is not present in the *stk* background. Bars = 50 μm.

(B) Analysis of *PMEI6* and *STK* expression in developing wild-type and *stk* siliques from 3 to 6 DAP. Measurements of relative mRNA levels indicate low expression levels of *PMEI6* in the absence of STK. Error bars represent the propagated error value of three replicates. **, Wilcoxon signed rank test, $P < 0.05$.

(C) *stk* mucilage release phenotype is complemented by *35S:PMEI6.* Bar = 100 μm.

(D) ChIP enrichment tests by qRT-PCR show that STK-GFP binds to the selected regions of *PMEI6* containing CArG-boxes 1, 2, and 4. Fold enrichment was calculated against the signal in the wild type. Error bars represent the propagated error value using three replicates. Binding of STK to a CArG-box in the *VERDANDI* promoter (VDDcarg3; see Methods) was used as the positive control. Schematic representation of the locations of putative CArG-boxes in the *PMEI6* locus is included. Five MADS recognition motif CArG-boxes are present. A ChIP enrichment assay showed that STK binds to two CArG-box regions (asterisk). Gray box, exon; triangles, CArG-boxes.

might influence the glucomannan content in Arabidopsis mucilage by whole-mount immunolabeling using the monoclonal antibody LM21, which binds to heteromannan polysaccharides. In wild-type water-imbibed seeds, LM21 labeled a combination of intense rays originating from the top of columellae and showed diffuse labeling between rays (Figure 6A). In wild-type EDTA-treated seeds, no LM21 signal was observed (Figure 6B). Interestingly, *stk* EDTA-extruded seeds showed irregular labeling, with strongly labeled regions in the outer layer of the adherent mucilage (Figure 6D).

Our data suggest that loss of *STK* influences the spatial distribution of glucomannans in the adherent mucilage.

STK Affects Mucilage Content and Composition

To find out if *stk* mutation affected the organization of the different polysaccharides within the mucilage secretory cells, we performed a sequential extraction of mucilage-containing polysaccharides (vigorously extracted using a vortex; see Methods), followed by the determination of their monosaccharide composition using gas-liquid chromatography (Supplemental Table 1). Following water imbibition, the total sugar content of *stk* seeds was very low, representing ~5% of that of wild-type water-extracted mucilage. However, compositional analysis of this fraction showed that the water-soluble fractions of both *stk* and wild-type consisted predominantly of rhamnose (Rha) and galacturonic acid (GalA) and that their compositions were very similar. After 0.2 M NaOH extraction, the total sugar content from *stk* seeds (115.6 nmol/mg) was greater than that obtained with the wild type (96.7 nmol/mg). In the wild-type seeds, 0.2 M NaOH-soluble mucilage represented ~42% of total mucilage, whereas in *stk*, this was increased to >70%. This additional quantity probably originated from mucilage that did not extrude with water. In this fraction, a substantial increase of both Rha and GalA contents in *stk* was observed. Finally, the 2 M NaOH extraction showed very little difference in terms of mucilage content from wild-type and *stk* seeds. The total amount of sugars across all three fractions was reduced to <70% in *stk* seeds with respect to wild-type seeds. Appreciable differences were noted in their total contents of GalA (~41 and ~37% in wild-type and *stk* seeds, respectively) and Rha (~31 and ~35%, in wild-type and *stk* seeds, respectively). We concluded that *stk* mutation affected the organization/distribution of mucilage-containing polysaccharides in both the water-soluble and 0.2 M NaOH-soluble fractions.

Transcriptional Network Controlling Pectin Modification in Mucilage Secretory Cells

Since STK is a transcription factor involved in the differentiation and function of the cell wall of the outermost seed coat layer, we investigated the genetic interaction between *STK* and other genes

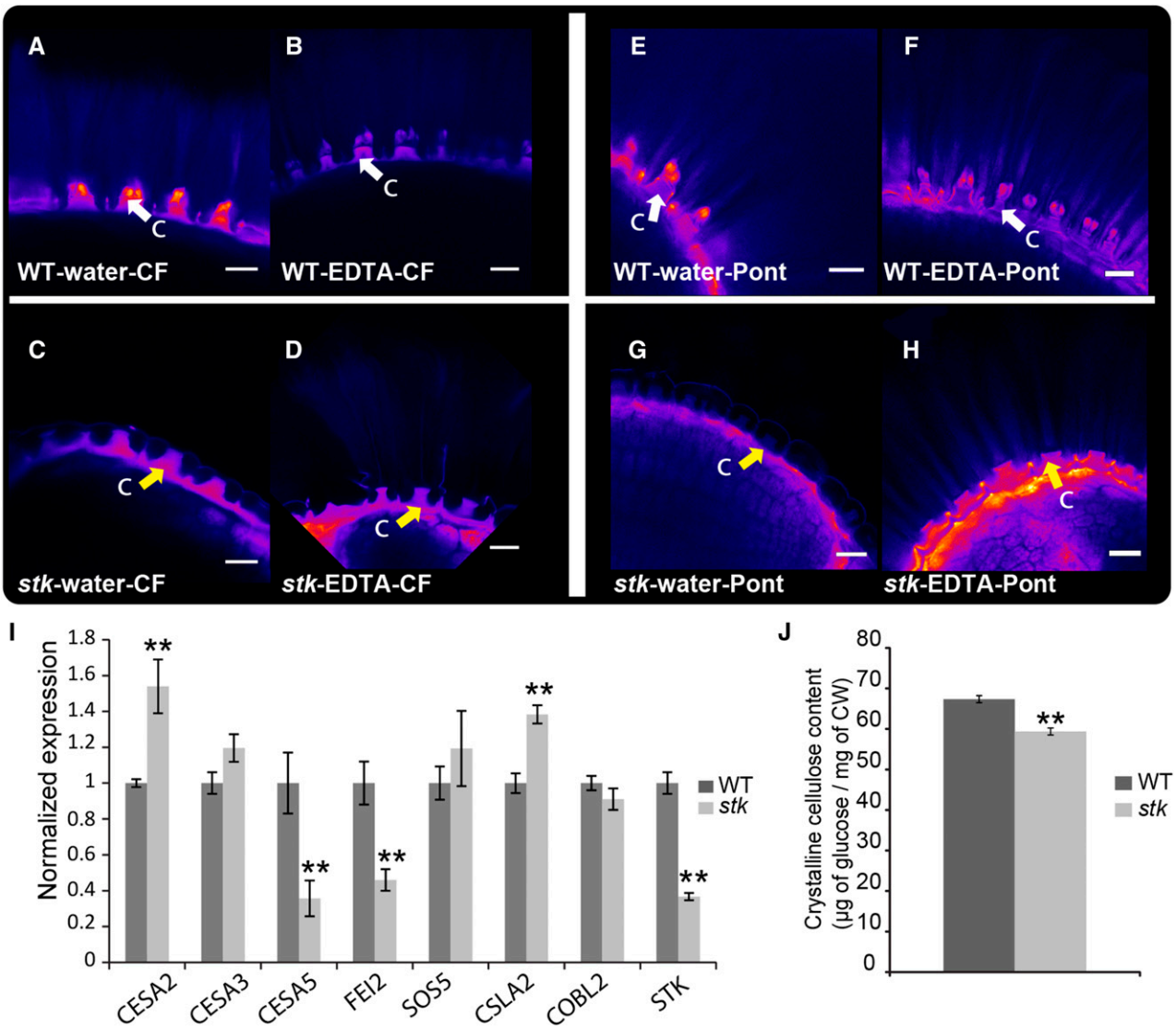

Figure 5. STK Affects the Cellulose That Connects Mucilage to the Seed.

(A) to **(H)** In situ localization of crystalline cellulose (blue signal) in wild-type (**[A]**, **[B]**, **[E]**, and **[F]**) and *stk* (**[C]**, **[D]**, **[G]**, and **[H]**) seeds. Detection of β-glycans with Calcofluor White (**[A]** to **[D]**) and crystalline cellulose by Pontamine (**[E]** to **[H]**) in water-imbibed (**[A]**, **[C]**, **[E]**, and **[G]**) and EDTA-imbibed seeds (**[B]**, **[D]**, **[F]**, and **[H]**). White arrows point out the columellae. Note the lack of tangential cell wall remnants on the tips of the columellae in *stk* seeds (marked with yellow arrows). C, columella. Bars = 20 μm.

(I) qRT-PCR analysis of *CESA2*, *3*, and *5*, *FEI2*, *SOS5*, *CBL2*, and *CSLA2* expression in developing siliques of wild-type and *stk* plants from 3 to 6 DAP. Relative mRNA levels are shown, with wild-type levels set to 1. Error bars represent the propagated error value using three replicates. **, Wilcoxon signed rank test comparing wild-type and mutant values, $P < 0.05$.

(J) Crystalline cellulose content is decreased in the *stk* mutant. Crystalline cellulose content from whole seed extracts was determined by the Updegraff (1969) method. Error bars represent SD ($n = 5$). **, Wilcoxon signed rank test, $P < 0.01$.

playing roles in mucilage secretory cell function, including mucilage hydrophilic properties and extrusion, pectin metabolism, and seed coat differentiation. For our analysis, we focused on *LEUNIG HOMOLOG/MUCILAGE MODIFIED1* (*LUH/MUM1*; Huang et al., 2011), MYB61 (Penfield et al., 2001), β-galactosidase-encoding MUM2 (Dean et al., 2007), subtilisin-like serine protease-encoding SBT1.7 (Rautengarten et al., 2008), transmembrane E3 ubiquitin ligase-encoding *FLYING SAUCER1* (*FLY1*) (Voiniciuc et al., 2013), and a member of the class III peroxidase family, *PEROXIDASE36* (*PER36*). Both SBT1.7 and FLY1 are required for correct methylesterification and extrusion of mucilage, while PER36 is active in the outer primary cell wall and generates reactive oxygen species that may degrade rhamnogalacturonan-I and/or HG during pectin secretion. In addition, *per36* mutant seeds show impaired mucilage defects that resemble those of the *sbt1.7* and *pmei6* mutants (Kunieda et al., 2013). The expression of these

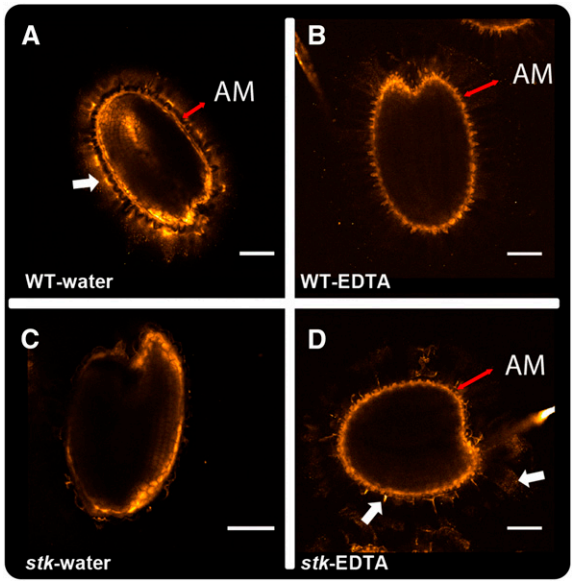

Figure 6. STK Mucilage Displays an Altered Pattern of Glucomannan Localization.

Localization of glucomannan in adherent mucilage released from wild-type (**[A]** and **[B]**) and *stk* (**[C]** and **[D]**) water- and EDTA-imbibed seeds upon LM21 monoclonal antibody staining. White arrows point out the presence of heteromannan in the adherent mucilage. AM, adherent mucilage. Bars = 20 μm.

genes was analyzed by qRT-PCR in developing wild-type and *stk* siliques (Supplemental Figure 3A). *LUH/MUM1*, *MYB61*, *MUM2*, and *SBT1.7* transcript levels were increased in the *stk* mutant, suggesting that STK could act as a repressor at this specific stage of development. However, ChIP assays revealed that STK did not directly bind the corresponding CArG-containing regions of these genes (Supplemental Figure 3B).

The transcriptional regulators GL2 and LUH/MUM1 have also been proposed to control *PMEI6* expression (Saez-Aguayo et al., 2013). To test if *STK* is controlled by LUH/MUM1 and GL2, we analyzed the expression of *STK* in developing siliques of *luh/mum1* and *gl2* mutants. Interestingly, *STK* transcript abundance was increased in the *luh/mum1* mutant (Supplemental Figure 3C), suggesting a reciprocal repressive interaction between STK and LUH/MUM1. Expression analysis of *STK* in *gl2* developing siliques revealed no change in *STK* expression (Supplemental Figure 3C), suggesting that GL2 is not involved in controlling *STK* expression.

DISCUSSION

The Role of STK in Seed Development Includes Modification of the Cell Wall Structure

Many cell wall-modifying enzymes, such as expansins and xyloglucan endotransglycosylases, and pectin modifying enzymes, including PMEs and PMEI proteins, play roles in cell wall reorganization. Although the corresponding genes have been found downstream of transcription factors controlling organogenesis and differentiation (Yant et al., 2010; Schlereth et al., 2010), the molecular and genetic mechanisms connecting differentiation and cell wall modification is still largely unknown.

Here, we provide an example of how homeotic transcription factors might be directly involved in cell wall differentiation and reorganization. The morphology of the outer cell layer of *stk* mutant seeds appears similar to that of the wild type; however, using biophysical technologies, such as AFM assays, we show that the *stk* seed coat epidermal cells are stiffer than those of the wild type (Figure 2C; Supplemental Figure 2). Our results suggest that alterations in the biophysical properties of the cell wall as described in this work influence the mechanical rupture of the seed coat upon water imbibition and the extrusion of mucilage during seed germination. This might be due to the reinforcement of pectin structures through the activation of PME activities and resultant formation of Ca^{2+} cross-links and/or to the many other modifications occurring during the development of the seed coat in the *stk* mutant. In concordance with our observations, Peaucelle and coworkers showed that PME activity influences the stiffness of the cell wall thereby controlling tissue growth and the emergence of organ primordia (Peaucelle et al., 2008, 2011). The use of innovative biophysical applications, such as AFM, will allow more detailed investigations of the effect of single or multiple changes in cell wall structures that affect cell wall functionality.

The *stk* phenotype is consistent with previous observations by Penfield and colleagues (2001), who showed that germination is compromised in mutants that show an alteration in mucilage release under drought conditions, which supports the importance of seed mucilage as a natural hydrogel and efficient absorber of water. Alterations in metabolite accumulation, specifically alterations in flavonoid pigmentation, can also affect seed germination (Debeaujon et al., 2000). Debeaujon et al. (2000) investigated the influence of the seed coat structure on seed dormancy, germination, and longevity and found that most mutants with altered flavonoid pigmentation, including *ban* and *tt8*, exhibited earlier germination. Recently, it has been demonstrated that *STK* plays a pivotal role in the control of anthocyanidin accumulation in the seed coat by negatively regulating *TT8* and *BAN* (Mizzotti et al., 2014). We therefore hypothesize that the altered germination properties of *stk* mutant seeds can be attributed to changes in the seed coat structures leading to altered water absorption, mechanical resistance, or both as a result of alterations in mucilage and PA properties.

STK Is a Major Regulator of PMEI6 Activity in Seed Coat Epidermal Cells

Modifications occurring in the cell wall and in mucilage components such as pectin methylesterification/demethylesterification have an effect on cell wall physical properties (Seymour and Knox, 2002). These modifications were recently shown to be crucial for adherent mucilage extrusion properties of Arabidopsis mucilage secretory cells (Saez-Aguayo et al., 2013; Voiniciuc et al., 2013). Similar to findings reported for the Arabidopsis *pmei6* mutant (Saez-Aguayo et al., 2013), we found no labeling of highly methylesterified HG in *stk* seeds (Figures 3G and 3H). This observation suggests that STK promotes mucilage release by modulating PME activity, which was also confirmed by the comparative analysis of PME activity in protein extracts of *stk* and wild-type seeds (Figures 3I and 3J).

Together, these results provide evidence that transcription factors controlling organ differentiation, such as the homeotic MADS domain factor STK, directly control key cell wall biosynthetic processes, such as HG methylesterification.

We also showed that the transcript levels of other regulators of the pectin maturation pathway during seed coat epidermal cell development such as *MYB61*, *MUM2*, *LUH/MUM1*, and *SBT1.7* are increased in the *stk* background (Supplemental Figure 3A). The *pmei6* and *sbt1.7* mutants both display a low level of methylesterification of HG and high PME activities when compared with the wild type (Saez Aguayo et al., 2013). The expression of *PMEI6* and *SBT1.7* in the *stk* mutant was lower and higher, respectively, compared with the wild type. This finding could indicate a compensatory effect on global PME activity. However, the finding that PME activities are increased in the *stk* mutant indicates that this altered activity is primarily influenced through the *PMEI6* pathway.

We propose a dual role for *STK* in the modulation of this pathway, first with *MUM2*, *MYB61*, *LUH/MUM1*, and *SBT1.7* as downstream targets (although it remains unclear if this occurs via direct repression or via activation of an intermediary inhibitor) and second by direct control to promote *PMEI6* expression. How alterations in the cell wall result in altered organ nanomechanics is still unknown. It may be reasonable to expect that the methylesterification status of pectins could modify the biophysical properties of the cell wall, since we have presented evidence that STK plays also a critical role in cell wall stiffening (Figure 2C). Future experiments will therefore be focused on determining the nature of the response of other plant organs that manifest dramatic cell wall changes during organogenesis to such coordinated genetic and biochemical events.

STK Modulates the Transcriptional Network Involved in Mucilage Packaging and Organization

Cellulose participates in the attachment of the adherent mucilage (Sullivan et al., 2011). Observations made on *stk* seeds treated with EDTA, which sequesters divalent cations (e.g., Ca^{2+}) and disrupts the cross-linking of pectins, showed that EDTA facilitated the release of *stk* mucilage within the seed epidermal cell wall. However, we observed no tangential cell wall remnants present on the columella tips and no labeling of cellulose structures with Calcofluor and with Pontamine Fast Scarlet 4BS (a generic stain for β-glucan and a cellulose-specific dye, respectively). Quantification of crystalline cellulose indeed revealed a significantly lower amount in *stk* seeds compared with the wild type (Figure 5J). Thus, our cellulose staining assays are consistent with the quantification data. We hypothesize that the reduction in cellulose found in the *stk* mutant might result from the loss of cellulose microfibrils, which may be decreased in the adherent mucilage of *stk*.

Our data also establish a role for STK in the control of cellulose deposition in seed coat epidermal cells. The final metabolic step of cellulose biosynthesis is driven by CESAs that tend to heterodimerize and generate an array of cellulose synthase complexes with specialized functions in different developmental contexts (Mendu et al., 2011). Our data show that *CESA5* transcript levels are markedly decreased in the *stk* mutant, while levels of *CESA3* (which is also involved in mucilage cellulose synthesis; Griffiths et al., 2015) were almost the same as in the wild type (Figure 5I). CESA5 and the Leu-rich receptor-like kinase FEI2 on one hand and the fasciclin-like arabinogalactan protein SOS5 on the other control mucilage adherence independently (Griffiths et al., 2014). While CESA5 and FEI2 are thought to do this by influencing cellulose biosynthesis, recently it was discovered that SOS5 mediates mucilage adherence through pectin organization, not cellulose (Griffiths et al., 2014). We found low *FEI2* mRNA levels in *stk* concomitantly with the decrease in *CESA5* (Figure 5I). Together with CESA5, other cellulose synthases like CESA2 affect radial cell wall thickening and the formation of the columellae

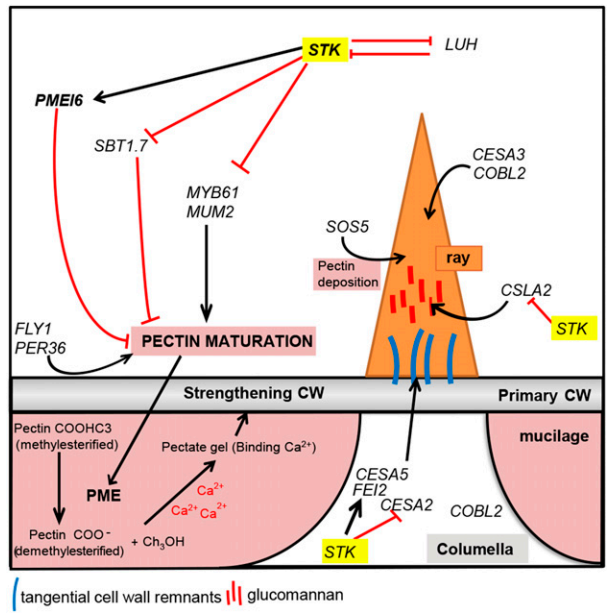

Figure 7. Model of the Central Role of STK in the Differentiation of Cell Wall of the Seed Coat Epidermal Cells.

The transcription factor STK regulates a complex regulatory network involving pectin maturation and cellulose deposition, driving the strengthening of the cell wall in the seed coat. STK controls the methylesterification status of the cell wall in the seed coat by repressing PME activity. STK represses genes involved in pectin maturation, including *LUH/MUM1*, *MYB61*, *SBT1.7*, and *MUM2*. As a transcription factor, LUH/MUM1 appears to antagonize STK function since each represses the other's activity. At the same time, STK directly promotes expression of the inhibitor *PMEI6*. This could explain the low *PMEI6* transcript levels and higher PME activity in *stk* seeds. This results in higher levels of demethylesterified HG, thereby exposing more negative charges that are involved in Ca^{2+} binding that might, directly or indirectly, strengthen the cell wall. The effects of induced stiffness in the seed coat might delay primary cell wall rupture with the described consequences for mucilage swelling. STK may play a parallel role in the positive regulatory control of cellulose biosynthesis in the mucilage ray via the *FEI2-CESA5* pathway. STK directly controls *CESA5* but does not induce changes in *SOS5*, *CESA3*, and *COBL2* expression. STK negatively influences glucomannan deposition in the adherent mucilage by repressing *CSLA2* regulation. STK controls cellulose deposition in the columellae and the radial cell wall promoting the expression of *CESA5* and repressing *CESA2*. STK promotes cellulose deposition to fulfill the need for a structural link required for the assembly/organization of pectin in the seed coat epidermal cell wall. The formation of this matrix may require the pectin matrix to be organized around cellulose rays in the columellae.

(Mendu et al., 2011). We found *CESA2* relative expression to be enhanced in the *stk* mutant. The role of COBL2 (found to be highly coexpressed with *FEI2*) in multiple aspects of secondary cell wall deposition in mucilage secretory cells, including ray formation, radial cell wall thickening, and the formation of the columellae, has recently been studied (Ben-Tov et al., 2015). That the levels of *SOS5* and *COBL2* were unaffected in the *stk* mutant suggests that STK-controlled cellulose deposition occurs via the control of *FEI2-CESA5* and is independent of *COBL2* and *SOS5.*

The glucomannan synthase-encoding gene *CSLA2* also affects cellulose deposition by controlling the way glucomannan is deposited in the external domain of adherent mucilage (Yu et al., 2014). We found altered glucomannan localization in *stk* seeds, with the presence of strongly labeled regions in the outer layer of the adherent mucilage (Figure 6D). Concomitantly, we found increased transcripts levels of *CSLA2* in *stk* compared with the wild type. Therefore, it seems that STK could influence adherent mucilage spatial organization, and this could involve altered glucomannan deposition via repression of *CSLA2.* Notably, our monosaccharide composition analysis showed that the *stk* mutation affected the organization/distribution of mucilage-containing polysaccharides (Supplemental Table 1). Several genes affecting mucilage adhesion have been recently discovered: *MUCILAGE-RELATED10* (affecting galactoglucomannan synthesis), *MUCILAGE-RELATED21* (implicated in the addition of xylan branches to mucilage polysaccharides), and *IRREGULAR XYLEM14* (involved in the production of xylan) (Voiniciuc et al., 2015b, 2015a). Future studies are needed to clarify the effect of STK on glucomannan, galactoglucomannan, and xylan cross-links with cellulose and other mucilage components and the resulting influences on Arabidopsis mucilage structure.

Taken together, our observations suggest that STK is involved in modulating the structure of adherent mucilage, regulating the expression of genes involved in (1) the degree of methylesterification of HGs, (2) controlling the adherence of mucilage to seed epidermis through cellulose deposition, and (3) altering the association between glucomannan and mucilage matrix. To date, the prevailing model of the cell wall assumes that a cellulose-hemicellulose network is embedded in a pectin matrix (reviewed in Fry, 2011). The mechanisms of assembly between pectins and the cellulose-hemicellulose network, which ultimately determines the relative strength of the tissue, are still unclear (reviewed in Cosgrove, 2014). Interestingly, recent studies have highlighted the existence of a critical relationship between celluloses, hemicelluloses, and pectins at the levels of the synthesis and deposition of these polymers, which affects the correct function of the seed coat (Griffiths et al., 2015, 2014). Given the data presented in this work, we propose that STK plays a pivotal role in the coordination of these processes.

Future Perspectives in Plant Development: Differentiation Patterns Are Connected to Cell Wall Alterations

Recent studies have highlighted the importance of methylesterification of cell wall pectins in determining a variety of important biological functions such as cell elongation, fruit ripening, and mechanical strength of supporting stems (Peaucelle et al., 2012; Hongo et al., 2012; Giovannoni, 2004).

Therefore, genetic and biochemical processes involved in cellulose-pectin matrix biosynthesis are critical in determining organ growth. In this study, genetic, biophysical, and biochemical approaches have been used to define how PME activity is fine-tuned in seed coat epidermal cells. Previous observations showed that the *stk* mutant displays a reduced seed size phenotype (Pinyopich et al., 2003). The question therefore arises as to whether *STK* control of HG demethylesterification could regulate seed growth either completely or at least in part. From a mechanistic point of view, a large number of negatively charged carboxyl groups on poorly methylesterified HG in the *stk* mutant could enhance Ca^{2+} cross-linking between pectins and influence the elasticity and porosity of cell wall matrix properties, and thus affect the ratio of growth during differentiation.

Based on our results, we propose a model (Figure 7) in which the maintenance of cell wall integrity throughout seed development, which is essential for correct seed coat biogenesis, is under control of the master developmental regulator STK. This represents a direct relationship between a differentiation process and the molecular mechanisms that underlay the properties related to mechanical stress responses in a tissue, in this case the seed coat. The studies presented here suggest that seed coat properties such as stiffness can be fine-tuned by genetic factors, thus influencing processes including primary cell wall rupture, mucilage swelling, and testa rupture under water-limiting conditions. These processes are central for seed germination and are of enormous importance for agriculture. Furthermore, this report highlights how changes in the expression of a master developmental regulator affect seed properties, underlining the important role these transcription regulators might have in the evolution of a species or during domestication by humans.

METHODS

Plant Material and Growth Conditions

Arabidopsis thaliana wild-type (ecotype Columbia) and *stk* plants were grown at 22°C under short-day (8 h light/16 h dark) or long-day (16 h light/8 h dark) conditions under continuous fluorescent illumination of 90 to 110 μmol m^{-2} s^{-1}. Arabidopsis *stk* seeds were kindly provided by M. Yanofsky. The *stk-2* allele contains a 74-nucleotide insertion near the splice site of the third intron (Pinyopich et al., 2003). The marker line pSTK:STK-GFP used in this work is described in Mizzotti et al. (2014). The *pPMEI6:PMEI6-GFP* marker line and the mutants *pmei6-1* (SM_3.19557), *35S:PMEI6* (pmei6OX-21), *luh-3* (SALK_107245C), and *gl2-6* (SM_3.16350) (Saez-Aguayo et al., 2013) were kindly provided by the Helen North Lab, Institut National de la Recherche Agronomique (INRA).

PCR-Based Genotyping

Identification of the *stk* and wild-type alleles was performed as described by Mizzotti et al. (2014).

Morphological Analysis

For mucilage release, whole seeds were stained by shaking in a 0.01% (w/v) ruthenium red (Sigma-Aldrich) solution for 90 min. Seeds treated with EDTA (0.5 M) were imbibed for 2 h before staining with ruthenium red. After staining, samples were rinsed in deionized water prior to visualization according to Durand et al. (2009). Seeds were observed and photographed

using a stereomicroscope. For mucilage extrusion, scanning electron microscopy was performed on wild-type and mutant seeds before and after imbibition. Dry seeds were maintained at 37°C overnight before proceeding with the analysis. Imbibed seeds were air dried overnight on filter paper and then treated the same as dry seeds. Dried and imbibed seeds were gold coated using a sputter coater (SEMPREP2; Nanotech) and observed with a LEO 1430 scanning electron microscope (LEO Electron Microscopy). For the morphological analysis of seed coat differentiation, wild-type and *stk* seeds at different stages of development were fixed as previously described (Ambrose et al., 2000). Sections (8 μm) were stained in 0.5% (w/v) Toluidine blue O. A Zeiss Axiophot D1 microscope equipped with differential interface contrast optics was used for observation, and images were recorded with an Axiocam MRc5 camera (Zeiss) using the Axiovision program (version 4.1).

Germination Tests on Polyethylene Glycol

Seeds from three independent batches of *stk* and wild-type plants grown side-by-side under identical environmental conditions were harvested on the same day. The seeds were placed on paper discs moistened with 1 mL water or PEG 8000 solution from 12 to 25% concentration (Sigma-Aldrich), sealed in Petri dishes, and stratified for 3 d at 4°C. Seeds were scored as germinated when testa rupture preceding radicle protrusion was visible. Similar results were obtained with seed stocks from a second set of plants grown independently.

Quantitative Real-Time PCR Analysis

qRT-PCR experiments were performed on cDNA obtained from 3 to 6 DAP siliques. Total RNA was extracted using the LiCl method (Verwoerd et al., 1989). DNA contamination was removed using the Ambion TURBO DNA-free DNase kit according to the manufacturer's instructions. The treated RNA was reverse transcribed using the ImProm-II reverse transcription system (Promega). Diluted aliquots of the first-strand synthesis were used as templates in the qRT-PCR reactions containing the iQ SYBR Green Supermix (Bio-Rad). The qRT-PCR assay was conducted in triplicate in a Bio-Rad iCycler iQ Optical System (software version 3.0a). The relative transcript enrichment of genes of interest was calculated by normalizing against various housekeeping genes (*UBIQUITIN*, *ACTIN*, *PPA2*, and *SAND*; Hong et al., 2010). The $2^{-\Delta\Delta C}{}_{T}$ method (Livak and Schmittgen, 2001) was used to analyze the data. Primers used are listed in Supplemental Table 2.

Monosaccharide Compositional Analysis of the Different Mucilage-Enriched Fractions

Sequential extractions of different mucilage-enriched fractions were performed following the protocol developed by Huang et al. (2011). Briefly, 125 mg of seeds (wild-type or *stk*) was placed in 2-mL test tubes with 2 mL water for 2 h. Water-exposed seeds were then further sequentially extracted with 0.2 and 2 M NaOH and stored at 4°C. During this procedure, tubes were vortexed every 5 min for 5 s. The material collected was used for compositional monosaccharide analyses. Mild and strong alkaline solutions were neutralized with glacial acetic acid, dialyzed against water, and lyophilized. To determine the total sugar contents in each fraction, we followed the protocol described by Filisetti-Cozzi and Carpita (1991). A gas-liquid chromatography method (Nguema-Ona et al., 2006; York et al., 1985) was used to determine the monosaccharide content of the different mucilage-enriched fractions. Approximately 0.5 to 1 mg mucilage was hydrolyzed (2 M trifluoroacetic acid 110°C, 2 h), and the liberated monosaccharides were converted to methoxy sugars using 1 M methanolic HCl at 80°C for 24 h. Silylation was performed at 80°C (20 min) to produce trimethyl-silyl-glycosides, which were dissolved in cyclohexane. The derivatives were separated and analyzed in a Varian 3500 gas-liquid chromatograph equipped with a flame ionization detector and a 30 m × 0.25 mm (i.d.) HPS-MS column. The oven temperature was stabilized at 120°C for 2 min, ramped at 10°C/min to 160°C, then at 1.5°C/min to 220°C and finally at 20°C/min to 280°C. Myo-inositol (0.5 μmol) was used as the internal standard. Derivatives were identified based on their retention times and quantified by determination of their peak areas. Monosaccharides (Sigma-Aldrich) were used as standards to determine the retention times of the nine main monosaccharides found in the plant cell wall. Sugar composition was expressed as mole percentage for each monosaccharide. Error bars in the histograms represent the SD of the mean of two biological samples and two technical replicates per biological sample.

ChIP Assay

The genomic regions located 3 kb upstream of the ATG, 1 kb downstream of the stop codon, and in the exons and introns of the selected genes were analyzed in silico to identify CArG-box sequences (allowing up to one mismatch). ChIP experiments were performed as a modified version of a previously reported protocol (Gregis et al., 2008) using a GFP polyclonal antibody (Living Colors Polyclonal antibody raised in rabbit; Clontech; cat no. 632460). Enrichment of the target region was determined by qRT-PCR (iQ_ SYBR Green Supermix; Bio-Rad). This assay was conducted in triplicate using a Bio-Rad iCycler iQ optical system (software version 3.0a). For the binding of STK to the selected genomic regions, the enrichment of targets obtained from *stk/stk* pSTK:STK-GFP siliques (up to 6 DAP) was compared with the enrichment of the same targets from wild-type siliques. Fold enrichment was calculated using *ACTIN7* and previously reported formulae (Matias-Hernandez et al., 2010). To determine the efficiencies of the chromatin immunoprecipitations, we used the third CArG-box of *VDD* as a positive control (Matias-Hernandez et al., 2010). Three independent ChIP assays were performed. Sequences of the oligonucleotides used for ChIP analyses are listed in Supplemental Table 2.

PME Activity Assays

PME activity was determined in protein extracts by the release of methanol 85% esterified citrus fruit pectin (Sigma-Aldrich). Equal amounts of proteins (10 μg) were incubated in 300 mL of 30 mM sodium phosphate buffer with pH 6.5 to which 1% pectin and 0.03 units of alcohol oxidase were added (Sigma-Aldrich). The mixture was incubated for 1 h at 28°C. Thereafter, a mixture of 500 μL containing 20 mM 2,4-pentanedione in 2 M ammonium acetate and 50 mM acetic acid was added. After 15 min of incubation at 60°C, samples were directly cooled on ice and absorbance was measured at 412 nm. The methanol content was calculated as the amount of formaldehyde produced from methanol by alcohol oxidase (Klavons and Bennett, 1986), by comparison with a standard calibration curve. For PME activity measurement via radial gel diffusion assays, gels were prepared with 0.1% (w/v) of 85% esterified citrus fruit pectin, 1% (w/v) agarose, 12.5 mM citric acid, and 50 mM Na_2HPO_4, pH 6.5. Volumes of 15 mL gel were cast into agar plates and allowed to polymerize at room temperature. Equal protein samples (4 μg in 20 μL) were loaded in 4-mm-diameter wells. Plates were incubated at 28°C for 16 h. The gels were stained with 0.05% (w/v) ruthenium red for 45 min and destained with water (five times in 5 h).

The measurement of the diameter of the red-stained areas, resulting from the hydrolysis of esterified pectin, was performed with ImageJ software.

Crystalline Cellulose Quantification

Dry Arabidopsis seeds (20 mg) of wild-type and *stk* genotypes were frozen in liquid nitrogen and ground to a fine powder. Ground material was washed twice with 70% (v/v) ethanol (1.5 mL) by vortexing and pelleting (17,000*g* for 15 min), discarding the supernatant. The pellets were washed three times

with a 1:1 (v/v) methanol:chloroform solution (1.5 mL per wash) under the previous conditions. The pellets (at this step, total cell wall fractions) were completely dried. For each pellet, 1 mg was treated with 1.5 mL Updegraff reagent (acetic acid:nitric acid:water, 8:1:2 [v/v]; Updegraff, 1969) at 98°C for 30 min. Samples were cooled to room temperature and pelleted (17,000*g* for 15 min) to obtain crystalline cellulose. The supernatants were carefully removed, and the pellets were washed four times with 1.5 mL acetone and pelleted at 17,000*g* for 15 min. Samples were dried completely at room temperature. The resulting crystalline cellulose was hydrolyzed with 175 μL of 72% (w/w) sulfuric acid for 1 h at room temperature under 300 rpm agitation. After hydrolysis, water was added (425 μL). The resulting solution was used for Glc determination using the anthrone assay; 1 mL of 0.2% (w/v) anthrone solution in 75% H_2SO_4 was added to each tube. Tubes were vortexed and heated in boiling water for 5 min. Tubes were cooled on ice and kept in the dark to prevent photobleaching. Absorbance was read at 620 nm. A standard curve was made with Glc. Cellulose hydrolytic efficiency was tested using cellulose standards.

Cytochemical Staining and Immunolabeling Procedures

Bright-field microscopy was used to observe whole-mounted seeds stained with 0.05% (w/v) ruthenium red dye (Sigma-Aldrich) in deionized water for 15 min. After staining, the seeds were gently washed in deionized water and observed. Staining of β-glucans, including cellulose, was performed using Calcofluor White M2R (Sigma-Aldrich; 1 mg/mL) Pontamine Fast Scarlet 4 BS stain (synonym Direct Red 23; Sigma-Aldrich; 0.01% [w/v]) for 30 min in the dark (Andème-Onzighi et al., 2002). After having been gently washed in deionized water, seeds were observed using a microscope equipped with a UV lamp (excitation filter, 359 nm; barrier filter, 461 nm). Images were acquired with a Leica DFC 300 FX camera and fluorescence microscope. Laser scanning confocal microscopy was used to observe whole-mounted seeds labeled with either with monoclonal antibodies to homogalacturonan (catalog code LM19 and LM20) or to heteromannan (catalog code LM21) (Verhertbruggen et al., 2009; Plant Probes). Immunolabeling was performed according to Macquet et al. (2007) with minor modifications. Briefly, intact mature seeds were imbibed in water without shaking for 30 min at room temperature and then fixed with 4% (w/v) paraformaldehyde for 1 h. Seeds were subsequently incubated for 2 h at room temperature or overnight with the primary antibody diluted 10-fold in PBS containing 1% (w/v) BSA. They were then washed with PBS (three times, 3 min per wash) and finally incubated for 2 h at 37°C with the secondary goat anti-rat-IgG antibody coupled to fluorescein isothiocyanate (Sigma-Aldrich) diluted 1:5000 in PBS containing 1% (w/v) BSA. After washing in PBS (three times, 3 min per wash), seeds were mounted on slides. An antifading agent (Citifluor; Agar Scientific) was incorporated before examination. For the labeling of EDTA-treated seeds, a similar protocol was followed except that seeds were successively imbibed in water and EDTA. The lookup table of ImageJ software (http://rsbweb.nih.gov/ij/) was used for all labelings.

Measurement of the Elastic (Young's) Modulus of the Cell Wall by AFM and Analysis of Data

Developing Arabidopsis seeds were isolated from independent siliques of *stk* and the wild type at 2 and 11 DAP. After dissection, the silique was mounted on double-sided tape and the replum was gently removed with tweezers to detach seeds without damaging them. The tape was placed on the bottom of a Petri dish filled with water to prevent dehydration during AFM measurements. An optical microscope allowed us to position the AFM cantilever at the desired location on the seed epidermal surface for AFM scanning.

AFM is based on the ability of a small flexible element (the cantilever) to be bent when forced to indent a sample (Supplemental Figure 2A). Since the mechanical properties of the cantilever are known, those of the sample can be deduced. At the same time, AFM provides topographic maps (height maps, as shown in Supplemental Figures 2B and 2C) in which higher regions are depicted in lighter colors. During the scanning process, the AFM performed force-curve measurements on a square grid of points on the seed surface, and these force curves were stored for further processing. The force curves were fitted using the Sneddon model (see methods) to extract the apparent Young's modulus (E) of the seed cell wall (units are MPa). The results of the analysis of developing seeds at 2 DAP are shown in Figure 2C. Each square represents the average apparent Young's modulus per seed of over 300 force curves, with the associated SD.

A Bruker Catalyst atomic force microscope was used in the quantitative nanomechanical property mapping (QNM) mode that allows acquisition of AFM force curves on a two-dimensional grid of points. All the force curves are stored and can be extracted for fitting. We used Bruker cantilevers with a pyramidal tip (Scanasyst-air, nominal stiffness 0.4 N/m). The spring constant was calibrated before each experiment using the thermal tune mode and was found to be in the range 0.16 to 0.47 N/m. All measurements were done in water. The positioning of the cantilever on each seed was made using an upright Leica microscope (MacroFluo). We chose seeds that were well positioned on their side and placed the cantilever tip above the center. The 60 × 60-μm scans (for 2 DAP seeds) and 70 × 70-μm scans (for 11 DAP seeds) were performed using the default QNM parameters (a scan rate of 0.5 Hz per line, 128 × 128 pixels; ScanAsyst Auto Control On). The typical maximal force applied was 20 μN (for 2 DAP seeds) and 50 μN (for 11 DAP seeds because of higher stiffness values in this developmental stage), resulting in typical maximal indentation depths ranging from 0.1 μm (*stk*) to 0.4 μm (wild type) depending on the seed. The AFM force curves chosen for analysis were extracted from regions in the middle of centrally located cells (two to three successive box selections). The fit was applied using Bruker's NanoScope Analysis software. To extract the mechanical properties of the cell wall (Milani et al., 2011), we analyzed force displacement curves between contact and 100-nm depth. As the tip is pyramidal, we applied a Sneddon fit to the curves (Milani et al., 2014). Given that the Sneddon fit to the retraction curves was more robust than the fit to those of extension, we chose to analyze the retraction curves, and possible adhesion was taken into account. Only those fits with a coefficient of determination R^2 higher than 0.95 were considered (the majority). More than 300 curves per seed were analyzed, allowing the computation of an average apparent elastic modulus and SD for each seed. This modulus most likely accounts for the properties in the direction perpendicular to the cell wall (Milani et al., 2011).

Accession Numbers

Sequence data from this article can be found in the GenBank/EMBL data libraries under the following accession numbers: *STK*, At4g09960; GL2, At1g79840; LUH/MUM1, At2g32700; PMEI6, At2g47670; SBT1.7, At5g67360; *SOS5*, At3g46550; *CESA2*, At4g39350; *CESA3*, AT5G05170; *CESA5*, At5g09870; *FEI2*, At2g35620; *MYB61*, At1g09540; *CSLA2*, At5g22740; *COBL2*, AT3G29810; *FLY1*, AT4G28370; and *PER36*, AT3G50990.

Supplemental Data

Supplemental Figure 1. Differentiation of seed coat epidermal cells in the *stk* mutant.

Supplemental Figure 2. Preparation of atomic force microscopy measurements on live developing *stk* and wild-type seeds (related to Figure 2C).

Supplemental Figure 3. SEEDSTICK controls the transcriptional network required for pectin modification in mucilage secretory cells.

Supplemental Table 1. Monosaccharide distributions in mole percentage of carboxyl-reduced mucilage polysaccharides from seeds successively extracted with water, 0.2 M NaOH, and 2 M NaOH.

Supplemental Table 2. Primers used for ChIP-PCR and qRT-PCR experiments.

ACKNOWLEDGMENTS

We thank Edward Kiegle and Andrew Peter MacCabe for assistance in editing the manuscript and Ogier Surcouf for technical help. This work was supported by the International European Fellowship-METMADS project, the Centro Nazionale di Ricerca Italiano (Fondo IBF-AR-01-2014Mi), the EXPOSEED-RISE project, and the Università degli Studi di Milano (Ass. ricerca Tipo A-2015) to I.E.; the Cariplo Foundation (Seefruit Grant 2011-2257) to C.M.; the Institut Universitaire de France to A.B.; and the Coordination for the Improvement of Higher Education Personnel (CAPES) and EVO-CODE project to V.E.V. The Université de Rouen and le Réseau de Recherche VASI de Haute Normandie (France) are also acknowledged for their financial support to A.D.

AUTHOR CONTRIBUTIONS

I.E., C.M., E.N.-O., L.B., and L.C. designed the research. I.E., C.M., E.N.-O., L.B., V.E.V., N.D., M.G., and A.-S.K. performed the research. I.E., C.M., E.N.-O., and L.B. analyzed data. A.B., A.D., A.C.d.O., E.C. and L.C. contributed reagents/materials/analysis tools. I.E., C.M., E.N.-O., A.D., A.B., and L.C. wrote the article. All authors read and contributed to the finalization of the article.

Received June 13, 2016; revised August 22, 2016; accepted September 9, 2016; published September 13, 2016.

REFERENCES

Ambrose, B.A., Lerner, D.R., Ciceri, P., Padilla, C.M., Yanofsky, M.F., and Schmidt, R.J. (2000). Molecular and genetic analyses of the silky1 gene reveal conservation in floral organ specification between eudicots and monocots. Mol. Cell **5:** 569–579.

Andème-Onzighi, C., Sivaguru, M., Judy-March, J., Baskin, T.I., and Driouich, A. (2002). The reb1-1 mutation of Arabidopsis alters the morphology of trichoblasts, the expression of arabinogalactan-proteins and the organization of cortical microtubules. Planta **215:** 949–958.

Anderson, C.T., Carroll, A., Akhmetova, L., and Somerville, C. (2010). Real-time imaging of cellulose reorientation during cell wall expansion in Arabidopsis roots. Plant Physiol. **152:** 787–796.

Arsovski, A.A., Popma, T.M., Haughn, G.W., Carpita, N.C., McCann, M.C., and Western, T.L. (2009). AtBXL1 encodes a bifunctional beta-D-xylosidase/alpha-L-arabinofuranosidase required for pectic arabinan modification in Arabidopsis mucilage secretory cells. Plant Physiol. **150:** 1219–1234.

Baudry, A., Caboche, M., and Lepiniec, L. (2006). TT8 controls its own expression in a feedback regulation involving TTG1 and homologous MYB and bHLH factors, allowing a strong and cell-specific accumulation of flavonoids in *Arabidopsis thaliana*. Plant J. **46:** 768–779.

Ben-Tov, D., Abraham, Y., Stav, S., Thompson, K., Loraine, A., Elbaum, R., de Souza, A., Pauly, M., Kieber, J.J., and Harpaz-Saad, S. (2015). COBRA-LIKE2, a member of the glycosylphosphatidylinositol-anchored COBRA-LIKE family, plays a role in cellulose deposition in arabidopsis seed coat mucilage secretory cells. Plant Physiol. **167:** 711–724.

Boudon, F., Chopard, J., Ali, O., Gilles, B., Hamant, O., Boudaoud, A., Traas, J., and Godin, C. (2015). A computational framework for 3D mechanical modeling of plant morphogenesis with cellular resolution. PLOS Comput. Biol. **11:** e1003950.

Bueso, E., Muñoz-Bertomeu, J., Campos, F., Brunaud, V., Martínez, L., Sayas, E., Ballester, P., Yenush, L., and Serrano, R. (2014). ARABIDOPSIS THALIANA HOMEOBOX25 uncovers a role for Gibberellins in seed longevity. Plant Physiol. **164:** 999–1010.

Cosgrove, D.J. (2014). Re-constructing our models of cellulose and primary cell wall assembly. Curr. Opin. Plant Biol. **22:** 122–131.

Dean, G.H., Zheng, H., Tewari, J., Huang, J., Young, D.S., Hwang, Y.T., Western, T.L., Carpita, N.C., McCann, M.C., Mansfield, S.D., and Haughn, G.W. (2007). The Arabidopsis MUM2 gene encodes a beta-galactosidase required for the production of seed coat mucilage with correct hydration properties. Plant Cell **19:** 4007–4021.

Debeaujon, I., Léon-Kloosterziel, K.M., and Koornneef, M. (2000). Influence of the testa on seed dormancy, germination, and longevity in Arabidopsis. Plant Physiol. **122:** 403–414.

Durand, C., Vicré-Gibouin, M., Follet-Gueye, M.L., Duponchel, L., Moreau, M., Lerouge, P., and Driouich, A. (2009). The organization pattern of root border-like cells of Arabidopsis is dependent on cell wall homogalacturonan. Plant Physiol. **150:** 1411–1421.

Filisetti-Cozzi, T.M., and Carpita, N.C. (1991). Measurement of uronic acids without interference from neutral sugars. Anal. Biochem. **197:** 157–162.

Favaro, R., Pinyopich, A., Battaglia, R., Kooiker, M., Borghi, L., Ditta, G., Yanofsky, M.F., Kater, M.M., and Colombo, L. (2003). MADS-box protein complexes control carpel and ovule development in Arabidopsis. Plant Cell **15:** 2603–2611.

Francoz, E., Ranocha, P., Burlat, V., and Dunand, C. (2015). Arabidopsis seed mucilage secretory cells: regulation and dynamics. Trends Plant Sci. **20:** 515–524.

Fry, S.C. (2011). Plant cell walls. From chemistry to biology. Ann. Bot. (Lond.) **108:** viii–x.

Giovannoni, J.J. (2004). Genetic regulation of fruit development and ripening. Plant Cell **16** (suppl.): S170–S180.

Gómez-Mena, C., de Folter, S., Costa, M.M.R., Angenent, G.C., and Sablowski, R. (2005). Transcriptional program controlled by the floral homeotic gene AGAMOUS during early organogenesis. Development **132:** 429–438.

Gregis, V., Sessa, A., Colombo, L., and Kater, M.M. (2008). AGAMOUS-LIKE24 and SHORT VEGETATIVE PHASE determine floral meristem identity in Arabidopsis. Plant J. **56:** 891–902.

Griffiths, J.S., Šola, K., Kushwaha, R., Lam, P., Tateno, M., Young, R., Voiniciuc, C., Dean, G., Mansfield, S.D., DeBolt, S., and Haughn, G.W. (2015). Unidirectional movement of cellulose synthase complexes in Arabidopsis seed coat epidermal cells deposit cellulose involved in mucilage extrusion, adherence, and ray formation. Plant Physiol. **168:** 502–520.

Griffiths, J.S., Tsai, A.Y.-L., Xue, H., Voiniciuc, C., Sola, K., Seifert, G.J., Mansfield, S.D., and Haughn, G.W. (2014). SALT-OVERLY SENSITIVE5 mediates Arabidopsis seed coat mucilage adherence and organization through pectins. Plant Physiol. **165:** 991–1004.

Harpaz-Saad, S., McFarlane, H.E., Xu, S., Divi, U.K., Forward, B., Western, T.L., and Kieber, J.J. (2011). Cellulose synthesis via the FEI2 RLK/SOS5 pathway and cellulose synthase 5 is required for the structure of seed coat mucilage in Arabidopsis. Plant J. **68:** 941–953.

Haughn, G., and Chaudhury, A. (2005). Genetic analysis of seed coat development in Arabidopsis. Trends Plant Sci. **10:** 472–477.

Haughn, G.W., and Western, T.L. (2012). Arabidopsis seed coat mucilage is a specialized cell wall that can be used as a model for genetic analysis of plant cell wall structure and function. Front. Plant Sci. **3:** 64.

Hong, S.M., Bahn, S.C., Lyu, A., Jung, H.S., and Ahn, J.H. (2010). Identification and testing of superior reference genes for a starting pool of transcript normalization in Arabidopsis. Plant Cell Physiol. **51:** 1694–1706.

Hongo, S., Sato, K., Yokoyama, R., and Nishitani, K. (2012). Demethylesterification of the primary wall by PECTIN METHYLESTERASE35 provides mechanical support to the Arabidopsis stem. Plant Cell **24:** 2624–2634.

Huang, J., DeBowles, D., Esfandiari, E., Dean, G., Carpita, N.C., and Haughn, G.W. (2011). The Arabidopsis transcription factor LUH/MUM1 is required for extrusion of seed coat mucilage. Plant Physiol. **156:** 491–502.

Keegstra, K. (2010). Plant cell walls. Plant Physiol. **154:** 483–486.

Klavons, J.A., and Bennett, R.D. (1986). Determination of methanol using alcohol oxidase and its application to methyl ester content of pectins. J. Agric. Food Chem. **34:** 597–599.

Krizek, B.A., Bequette, C.J., Xu, K., Blakley, I.C., Fu, Z.Q., Stratmann, J., and Loraine, A.E. (2016). RNA-Seq links AINTEGUMENTA and AINTEGUMENTA-LIKE6 to cell wall remodeling and plant defense pathways in Arabidopsis. Plant Physiol. **171:** 2069–2084.

Kunieda, T., Shimada, T., Kondo, M., Nishimura, M., Nishitani, K., and Hara-Nishimura, I. (2013). Spatiotemporal secretion of PEROXIDASE36 is required for seed coat mucilage extrusion in Arabidopsis. Plant Cell **25:** 1355–1367.

Livak, K.J., and Schmittgen, T.D. (2001). Analysis of relative gene expression data using real-time quantitative PCR and the 2(-Δ Δ C (T)) method. Methods **25:** 402–408.

Lodish, H., Berk, A., Zipursky, A., Matsudaira, P., Baltimore, D., and Darnell, J. (2000). Molecular Cell Biology, (New York: W.H. Freeman).

Macquet, A., Ralet, M.-C., Kronenberger, J., Marion-Poll, A., and North, H.M. (2007). In situ, chemical and macromolecular study of the composition of *Arabidopsis thaliana* seed coat mucilage. Plant Cell Physiol. **48:** 984–999.

Matias-Hernandez, L., Battaglia, R., Galbiati, F., Rubes, M., Eichenberger, C., Grossniklaus, U., Kater, M.M., and Colombo, L. (2010). VERDANDI is a direct target of the MADS domain ovule identity complex and affects embryo sac differentiation in Arabidopsis. Plant Cell **22:** 1702–1715.

Mendu, V., Griffiths, J.S., Persson, S., Stork, J., Downie, A.B., Voiniciuc, C., Haughn, G.W., and DeBolt, S. (2011). Subfunctionalization of cellulose synthases in seed coat epidermal cells mediates secondary radial wall synthesis and mucilage attachment. Plant Physiol. **157:** 441–453.

Milani, P., Gholamirad, M., Traas, J., Arnéodo, A., Boudaoud, A., Argoul, F., and Hamant, O. (2011). In vivo analysis of local wall stiffness at the shoot apical meristem in Arabidopsis using atomic force microscopy. Plant J. **67:** 1116–1123.

Milani, P., Mirabet, V., Cellier, C., Rozier, F., Hamant, O., Das, P., and Boudaoud, A. (2014). Matching patterns of gene expression to mechanical stiffness at cell resolution through quantitative tandem epifluorescence and nanoindentation. Plant Physiol. **165:** 1399–1408.

Mizzotti, C., Ezquer, I., Paolo, D., Rueda-Romero, P., Guerra, R.F., Battaglia, R., Rogachev, I., Aharoni, A., Kater, M.M., Caporali, E., and Colombo, L. (2014). SEEDSTICK is a master regulator of development and metabolism in the Arabidopsis seed coat. PLoS Genet. **10:** e1004856.

Mizzotti, C., Mendes, M.A., Caporali, E., Schnittger, A., Kater, M.M., Battaglia, R., and Colombo, L. (2012). The MADS box genes SEEDSTICK and ARABIDOPSIS Bsister play a maternal role in fertilization and seed development. Plant J. **70:** 409–420.

Nguema-Ona, E., Andème-Onzighi, C., Aboughe-Angone, S., Bardor, M., Ishii, T., Lerouge, P., and Driouich, A. (2006). The reb1-1 mutation of Arabidopsis. Effect on the structure and localization of galactose-containing cell wall polysaccharides. Plant Physiol. **140:** 1406–1417.

North, H.M., Berger, A., Saez-Aguayo, S., and Ralet, M.-C. (2014). Understanding polysaccharide production and properties using seed coat mutants: future perspectives for the exploitation of natural variants. Ann. Bot. (Lond.) **114:** 1251–1263.

Peaucelle, A., Braybrook, S., and Höfte, H. (2012). Cell wall mechanics and growth control in plants: the role of pectins revisited. Front. Plant Sci. **3:** 121.

Peaucelle, A., Braybrook, S.A., Le Guillou, L., Bron, E., Kuhlemeier, C., and Höfte, H. (2011). Pectin-induced changes in cell wall mechanics underlie organ initiation in Arabidopsis. Curr. Biol. **21:** 1720–1726.

Peaucelle, A., Louvet, R., Johansen, J.N., Höfte, H., Laufs, P., Pelloux, J., and Mouille, G. (2008). Arabidopsis phyllotaxis is controlled by the methyl-esterification status of cell-wall pectins. Curr. Biol. **18:** 1943–1948.

Pelloux, J., Rustérucci, C., and Mellerowicz, E.J. (2007). New insights into pectin methylesterase structure and function. Trends Plant Sci. **12:** 267–277.

Penfield, S., Meissner, R.C., Shoue, D.A., Carpita, N.C., and Bevan, M.W. (2001). MYB61 is required for mucilage deposition and extrusion in the Arabidopsis seed coat. Plant Cell **13:** 2777–2791.

Pinyopich, A., Ditta, G.S., Savidge, B., Liljegren, S.J., Baumann, E., Wisman, E., and Yanofsky, M.F. (2003). Assessing the redundancy of MADS-box genes during carpel and ovule development. Nature **424:** 85–88.

Pourcel, L., Routaboul, J.-M., Kerhoas, L., Caboche, M., Lepiniec, L., and Debeaujon, I. (2005). TRANSPARENT TESTA10 encodes a laccase-like enzyme involved in oxidative polymerization of flavonoids in Arabidopsis seed coat. Plant Cell **17:** 2966–2980.

Rautengarten, C., Usadel, B., Neumetzler, L., Hartmann, J., Büssis, D., and Altmann, T. (2008). A subtilisin-like serine protease essential for mucilage release from Arabidopsis seed coats. Plant J. **54:** 466–480.

Saez-Aguayo, S., Ralet, M.-C., Berger, A., Botran, L., Ropartz, D., Marion-Poll, A., and North, H.M. (2013). PECTIN METHYLESTERASE INHIBITOR6 promotes Arabidopsis mucilage release by limiting methylesterification of homogalacturonan in seed coat epidermal cells. Plant Cell **25:** 308–323.

Schlereth, A., Möller, B., Liu, W., Kientz, M., Flipse, J., Rademacher, E.H., Schmid, M., Jürgens, G., and Weijers, D. (2010). MONOPTEROS controls embryonic root initiation by regulating a mobile transcription factor. Nature **464:** 913–916.

Seymour, G.B., and Knox, J.P. (2002). Pectins and Their Manipulation. (Oxford, UK: C.P. Blackwell Publishing).

Skinner, D.J., Hill, T.A., and Gasser, C.S. (2004). Regulation of ovule development. Plant Cell **16** (suppl.): S32–S45.

Sullivan, S., Ralet, M.-C., Berger, A., Diatloff, E., Bischoff, V., Gonneau, M., Marion-Poll, A., and North, H.M. (2011). CESA5 is required for the synthesis of cellulose with a role in structuring the adherent mucilage of Arabidopsis seeds. Plant Physiol. **156:** 1725–1739.

Tilly, J.J., Allen, D.W., and Jack, T. (1998). The CArG boxes in the promoter of the Arabidopsis floral organ identity gene APETALA3 mediate diverse regulatory effects. Development **125:** 1647–1657.

Updegraff, D.M. (1969). Semimicro determination of cellulose in biological materials. Anal. Biochem. **32:** 420–424.

Verhertbruggen, Y., Marcus, S.E., Haeger, A., Ordaz-Ortiz, J.J., and Knox, J.P. (2009). An extended set of monoclonal antibodies to pectic homogalacturonan. Carbohydr. Res. **344:** 1858–1862.

Verwoerd, T.C., Dekker, B.M., and Hoekema, A. (1989). A small-scale procedure for the rapid isolation of plant RNAs. Nucleic Acids Res. **17:** 2362.

Voiniciuc, C., Dean, G.H., Griffiths, J.S., Kirchsteiger, K., Hwang, Y.T., Gillett, A., Dow, G., Western, T.L., Estelle, M., and Haughn,

G.W. (2013). Flying saucer1 is a transmembrane RING E3 ubiquitin ligase that regulates the degree of pectin methylesterification in Arabidopsis seed mucilage. Plant Cell **25:** 944–959.

Voiniciuc, C., Günl, M., Schmidt, M.H.-W., and Usadel, B. (2015a). Highly branched xylan made by IRREGULAR XYLEM14 and MUCILAGE-RELATED21 links mucilage to Arabidopsis seeds. Plant Physiol. **169:** 2481–2495.

Voiniciuc, C., Schmidt, M.H.-W., Berger, A., Yang, B., Ebert, B., Scheller, H.V., North, H.M., Usadel, B., and Günl, M. (2015b). MUCILAGE-RELATED10 produces galactoglucomannan that maintains pectin and cellulose architecture in Arabidopsis seed mucilage. Plant Physiol. **169:** 403–420.

Western, T.L. (2012). The sticky tale of seed coat mucilages: production, genetics, and role in seed germination and dispersal. Seed Sci. Res. **22:** 1–25.

Western, T.L., Skinner, D.J., and Haughn, G.W. (2000). Differentiation of mucilage secretory cells of the Arabidopsis seed coat. Plant Physiol. **122:** 345–356.

Willats, W.G., Orfila, C., Limberg, G., Buchholt, H.C., van Alebeek, G.J., Voragen, A.G., Marcus, S.E., Christensen, T.M., Mikkelsen, J.D., Murray, B.S., and Knox, J.P. (2001). Modulation of the degree and pattern of methyl-esterification of pectic homogalacturonan in plant cell walls. Implications for pectin methyl esterase action, matrix properties, and cell adhesion. J. Biol. Chem. **276:** 19404–19413.

Windsor, J.B., Symonds, V.V., Mendenhall, J., and Lloyd, A.M. (2000). Arabidopsis seed coat development: morphological differentiation of the outer integument. Plant J. **22:** 483–493.

Yang, X., Baskin, J.M., Baskin, C.C., and Huang, Z. (2012). More than just a coating: Ecological importance, taxonomic occurrence and phylogenetic relationships of seed coat mucilage. Perspect. Plant Ecol. Evol. Syst. **14:** 434–442.

Yant, L., Mathieu, J., Dinh, T.T., Ott, F., Lanz, C., Wollmann, H., Chen, X., and Schmid, M. (2010). Orchestration of the floral transition and floral development in Arabidopsis by the bifunctional transcription factor APETALA2. Plant Cell **22:** 2156–2170.

York, W., Darvill, A., McNeil, M., Stevenson, T., and Albersheim, P. (1985). Isolation and characterization of plant cell walls and cell wall components. Methods Enzymol. **118:** 3–40.

Yu, L., Shi, D., Li, J., Kong, Y., Yu, Y., Chai, G., Hu, R., Wang, J., Hahn, M.G., and Zhou, G. (2014). CELLULOSE SYNTHASE-LIKE A2, a glucomannan synthase, is involved in maintaining adherent mucilage structure in Arabidopsis seed. Plant Physiol. **164:** 1842–1856.